MAGNETOHYDRODYNAMIC INDUCTION GENERATOR EXPERIMENTAL STUDY

FINAL TECHNICAL REPORT

APRIL 15, 1970

PREPARED FOR THE JET PROPULSION LABORATORY
UNDER CONTRACT NO. 952453

This work was performed for the Jet Propulsion Laboratory, California Institute of Technology, sponsored by the National Aeronautics and Space Administration under Contract NAS7-100.

UNIVERSITY OF ILLINOIS
BOX 4348
CHICAGO, ILLINOIS 60680

ACKNOWLEDGEMENT

The use of the facilities at the Argonne National Laboratory is gratefully acknowledged, along with the advice and encouragement of Dr. Michael Petrick of Argonne National Laboratory and Dr. David G. Elliott of Jet Propulsion Laboratory. Edward M. Spleha did most of the mechanical design and provided important advice. Ralph A. Esposito and Leonard M. Indykiewicz aided in the construction and operation of the facility.

Construction of much of the generator and facility was supported by the U.S. Air Force under Contract F33615-67-C-1375 with the Air Force Aero Propulsion Laboratory, Wright-Patterson Air Force Base, Ohio.

ABSTRACT

The results for an experimental study of a one-wavelength MHD induction generator operating on a liquid flow are presented. First the design philosophy and the experimental generator design are briefly summarized, including a description of the flow loop and instrumentation. Next the measurements without the fluid or fluid channel are presented, followed by the results obtained for the fluid flow without the magnetic field. Finally the various generator test results are presented. Included are normal operation when excited from the 60-hertz power line, and operation from the power line with the end coils shorted to reduce magnetic fringing. Both of these cases were also operated in the self-excited mode with external capacitors to supply the required reactive power. The harmonic content of the terminal voltage was measured, hypothetical accidents simulated, and two-wavelength tests performed.

TABLE OF CONTENTS

SECTION I

INTRODUCTION

The study of the MHD induction generator for liquid-metal power systems was started in 1962 when Jackson and Pierson [1]* first showed that the device was not practical with typical MHD plasmas but was attractive with liquid metals. The next step was to couple the induction generator with the first two-phase cycle, proposed earlier in 1962 by Elliott [2], and thus to obtain a feasible cycle utilizing a liquid flow in the generator and producing AC directly. Since then the two-phase cycle combined with the induction generator has been under consideration by many workers [3-8], and appears to be the closest to actual utilization [8].

In the past several years there has been considerable theoretical study of the induction generator [9-16], and the device is now much better understood. However, the value of these theoretical studies is limited because of the complexity of the device, so that it is not possible to develop a truly comprehensive analytical treatment and any design must rely to some extent on engineering judgements. The theoretical predictions are good at high slip values, where the individual loss mechanisms other than ohmic loss in the fluid play a small part in the total picture. However, at the low values of slip required for a highly-efficient generator these other loss terms become significant, because the ohmic loss is now proportionally much smaller, and result in discrepancies between the expected and the actual experimental performances [17].

In the light of the considerable recent theoretical progress, and the lack of equivalent experimental correlation, it was felt that a careful, detailed experimental program was required so that these relatively small but important discrepancies could be explained and corrections made in the theory and/or design practice. To this end, a generator has been designed and built to operate on an addition to the existing NaK flow loop at the Argonne National Laboratory.

In Section II the design philosophy, the experimental generator, and the facility are briefly presented. The design is described in more detail in a previous report [18], which also includes a summary of the theory. The experimental results are given in Section III. The magnetic field with no fluid and the fluid flow with no magnetic field are first measured. Then a series of generator measurements are summarized and discussed.

---

* Numbers in brackets references at the end of the report.

SECTION II

EXPERIMENTAL GENERATOR AND FACILITY

2.1 DESIGN PHILOSOPHY

The basic objective of this experimental program is to gain further understanding of the operation of the MHD induction generator, and in particular to examine the discrepancies between the expected and the actual performances at low slips. To this end it is desired:

1. To build a machine whose performance, whatever is may be, can be accurately predicted. This requires a simple design.

2. To do a careful, controlled experiment. This has not been adequately done previously because most earlier experiments were not capable of steady operation.

3. To design a generator capable of reaching a high enough slip, say s = -0.8 as shown by previous experiments [17], so that the losses which cause the discrepancies at small slips are no longer significant. This provides a check point on the performance.

4. To build a one-wavelength generator as this appears to be best for matching to a power cycle and system. The longer wavelength of the one-wavelength machine yields a stronger interaction between the fluid and the traveling field and a better power factor. However, more than one slot per phase per pole should be used to allow operation as both a single- and a multi-wavelength machine simply by reconnecting the coils and to obtain a better approximation to a pure traveling magnetic field.

5. To include provisions for a careful study of the end losses, which will be significant if proper corrections are not included in the design. This means that the machine must be capable of operation with and without both compensating poles and vanes in the end regions.

6. To wind the exciting coils in such a fashion that the current in each slot can be independently controlled, allowing grading of the winding for end studies and balancing the phases. This is accomplished by winding each coil around the back of the core so that each coil is in only one slot, and by including a tap 10% from the end of each coil.

7. To build a machine that is capable of self-excited operation as a generator. This is not only necessary for a practical machine

but, lacking a variable-frequency power source, it allows much greater experimental flexibility. It should also be capable of operation from a 60-hertz three-phase power line.

8. To include provision for operation with a two-phase (liquid and vapor) mixture as this is expected for practical power systems.

These above points formed the basic framework for this generator design.

To achieve the above major points, and to obtain the maximum amount of information from a single traveling-field structure or stator, a constant-field and fluid-velocity generator was chosen as this has more experimental flexibility than the variable-fluid-velocity generator with either constant or varying field velocity. More important, the variable-velocity machine would not yield the controlled experiment desired because of the interaction between the end and variable-velocity effects. It was felt that the major areas where information was required were end losses and operation with two-phase working fluids, and that it was preferrable to concentrate on points 1, 5, and 8 and leave variable field velocity for later experiments.

2.2 EXPERIMENTAL GENERATOR DESIGN

The main constraint on the size of the generator is the flow loop, and in particular the rating of the pump. It was decided to use initially the existing pump, rated at 250 gallons per minute at 82 psi. The generator is designed to use the full flow capacity of the pump only at the highest desired fluid velocity (slip), and to use a maximum of about 60 psi pressure drop across the generator. This allows leeway for pressure losses in the flow loop, the pressure wasted as lost kinetic energy into the storage tank, and the uncertainty in the actual pump performance since it has never been run at full flow.

The electrical constraints on the experimental generator are very loose. Three-phase, 60 hertz, 480 volt power is available with more than adequate capacity. The generator is driven through three single-phase variacs for control. Capacitors in parallel with the generator are used to reduce the reactive power load on the variacs and thus improve the regulation, and are required for self-excited operation. Operation at other frequencies is possible only self-excited, or with the addition of a variable-speed motor-generator set.

The practical constraints for obtaining an acceptable experimental performance are more subtle. Some of these were mentioned in Section 2.1. Further constraints are:

1. The viscous pressure drop must represent a small fraction of the total available pressure in order to model a practical generator. This is required both for acceptable efficiency and for a large field-fluid interaction where the electromagnetic force dominates over the viscous force. Otherwise a sharp Hartmann profile (or the equivalent for turbulent flow) will not be attained, and the ohmic losses in the boundary layers will be unreasonably large [9].

2. The generator height parallel to the magnetic field, $2a_f$, should be small to reduce the exciting ampere turns and power required because space for the winding is limited, but large to reduce the viscous loss. Also, a_f has to be larger than the wall and/or insulation thickness so that most of the field volume performs useful work, improving the power density and power factor. Finally, $2\pi a_f/\lambda << 1$ for an acceptable power density (slit channel), where λ is the wavelength.

3. The wavelength λ should be long for a strong interaction between the field and fluid, but short to reduce the viscous loss. The wavelength determines how much room is available for the exciting winding, and thus how many ampere turns and slots per phase per pole can be squeezed in.

4. The generator width c should be large so that the effects of the copper side walls and the current loops closing through them are small, but increasing the width decreases the maximum fluid velocity and thus the wavelength.

5. The stator design should be such as to minimize the effect of slot harmonics, which appear to have been important in previous experiments [19]. A design which allows their effect to be observed experimentally would be even better.

6. Conducting channel walls should be avoided because thier ohmic loss will be proportionally very large in a small generator (smaller ratio of generator volume to surface area). Also, the walls will be more sensitive to slot harmonics, which decrease away from the edge of the core. In order to avoid wall loss dominating the generator performance, hiding the very losses of interest in this experiment, and interfering with self-excited operation; it was decided to use a non-conducting fluid channel except for copper side bars to reduce the edge effects.

As can be seen from the above, the design of the experimental generator is not a trivial exercise because many of the constraints are contradictory.

2.2.1 Channel Design and Dimensions

A fluid channel is required to protect the stator and reduce the danger of leakage but, as mentioned, conducting channel walls should be avoided. Thus, it was decided to use a fiberglass*channel because fiberglass is less likely to crack and has a higher temperature rating. The minimum wall thickness a_i, 1/16 inch to avoid the danger of breakage, is chosen to minimize the required exciting ampere turns. With a channel this thin, it is assumed that the iron core is perfectly smooth and will be used to mechanically back up the channel and absorb all of the pressure force. (The channel was carefully tested at the maximum working pressure of 100 psi before its use with NaK.) Incidently, the core will probably be used for structural backup in a power

---

* The initial channel was lucite, but it was not possible to obtain a leak-free seal between the lucite and copper.

system to again reduce the required wall thickness, whether the wall is a conductor or an insulator.

In spite of the insulating top and bottom channel walls, conducting side walls are desired to facilitate the closing of the fluid current loops and thus increase the power density. This is accomplished by using copper side walls, as shown in Fig. 1. The completed channel including the compensating-poles regions is shown in Fig. 2. The copper bars are clamped so that they cannot be pushed out by the static pressure force, and have a lip which rests against the core so that they cannot be pulled into the channel by the $\vec{J} \times \vec{B}$ force or the dynamic pressure force. Leakage between the copper and the fiberglass is prevented by inserting the fiberglass into a slot in the copper. The copper extends into the region between the two cores, in spite of slightly increased ohmic losses, to provide additional sealing and, more important, to provide the mechanical strength to support the cores when they are clamped together.

The first dimension chosen was the height $a_f = 0.25$ cm, compared to the wall thickness of 0.159 cm. The choices for λ and s_{max}, the maximum attainable slip, are independent but together fix the other parameters and the generator performance. The relevant equations are $v_{max} = (1 - s_{max})f\lambda$, and $c = Q_{max}/2a_f v_{max}$, where f is 60 hertz and Q_{max} is the maximum flow rate of the pump. After several trials, the values $\lambda = 0.21$ m and $s_{max} = -0.8$ were selected, giving $c = 0.1393$ m. (In the actual generator c turned out to be about 0.1405 m because it was not feasible to control the width of the iron core precisely.)

The estimated power and pressure drops for this design are shown in Table I, where the equations for the slit-channel induction machine were used [9,10] with the design peak magnetic flux density $B = 0.4$ wb/m^2 and the appropriate NaK properties of $\sigma_f = 2.38 \times 10^6$ mhos/m, $\rho = 847$ kg/m^3, and $\eta = 4.68 \times 10^{-4}$ kg/m-sec. Only the traveling-field region is considered, perfect compensation for the ends is assumed, and the edge effects are ignored. In the table P_s is the power supplied by the fluid to the exciting winding (electrical output power when coil and core losses are ignored), P_m is the mechanical input power, Δp_{em} is the electromagnetic pressure difference, and R_e is the Reynolds number. The viscous pressure drop Δp_v is calculated using the friction factor for turbulent flow without a magnetic field [20] as the case with a magnetic field is not clearly documented [9].

The correction required for the non-flat velocity profile is shown in Table II. The Hartmann number M based on the rms magnetic flux density is 50.4, which is on the borderline of being too small. To see this, the ratio of δ^*, the distance the channel wall would have to be moved in to maintain the same volume flow rate if the velocity was constant at the maximum (center line) value, to a_f is calculated using an approximate turbulent boundary-layer solution [9]. Since for a Hartmann profile $\delta^*/a_f = 1/M$, this is used to calculate an effective M, M_{eff}, as far as the fluid ohmic losses due to the non-flat profile are concerned. The effect of this is to multiply P_m by the profile Factor F_m, which takes the extra ohmic losses into account, but to leave P_s unchanged [9]. The increase in P_m is 7% at s_{max}, with larger increases as s approaches zero.

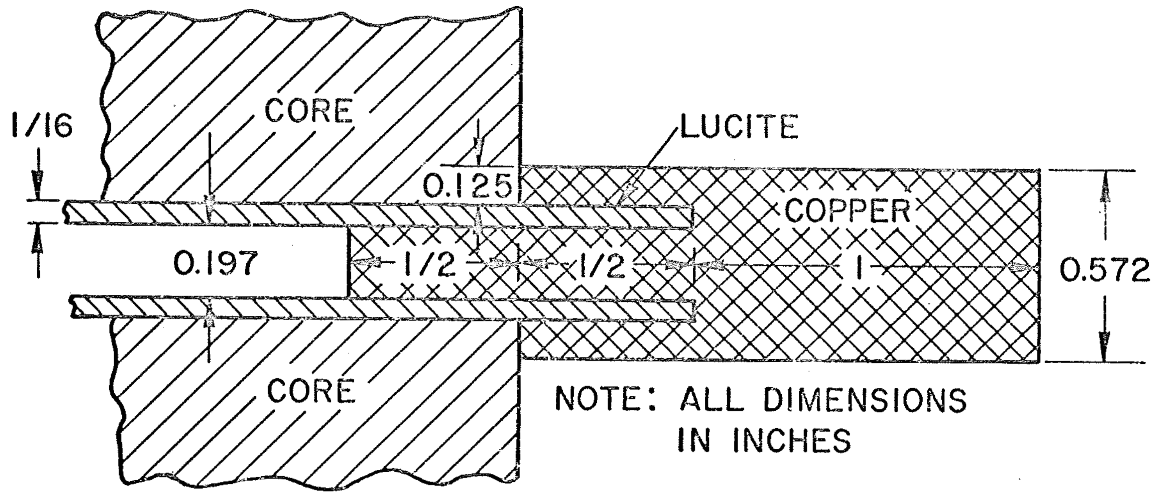

Fig. 1. Detail of channel construction.

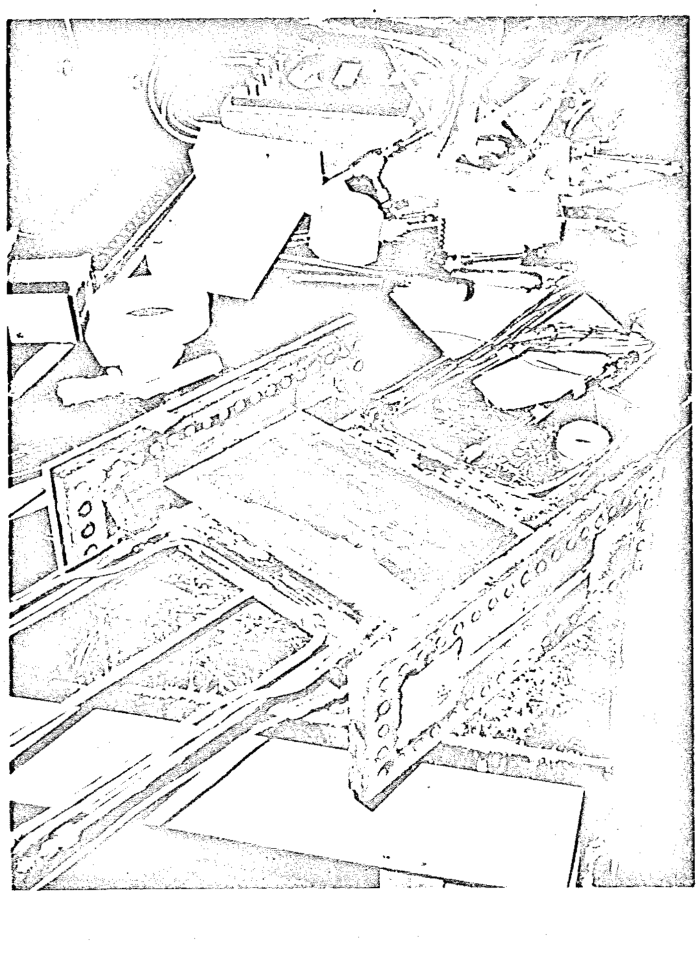

Fig. 2. Completed channel.

TABLE I. Powers and pressure drops for the traveling-wave region.

Parameters	Units			
s		-0.8	-0.5	-0.3
v	m/sec	22.7	18.9	16.4
B	wb/m^2	0.4	0.4	0.4
P_s	watts	3570	2230	1340
P_m	watts	6420	3350	1740
Δp_{em}	psi	59.1	36.9	22.2
R_e		3.96×10^5	3.30×10^5	2.86×10^5
Δp_v	psi	9.4	6.8	5.2
Δp_{total}	psi	68.5	43.7	27.4

Table II. Velocity profile corrections.

Parameter			
s	-0.8	-0.5	-0.3
M	50.4	50.4	50.4
R_e	3.96×10^5	3.30×10^5	2.86×10^5
δ^*/a_f	0.062	0.056	0.05
M_{eff}	16.1	17.9	20
F_m	1.069	1.084	1.108

One other point is to estimate the effect of the copper side walls or the finite generator width on the performance. The peak current in the side walls, assuming that all of the fluid current flows in them and that their presence does not change the fluid current from the infinite-width value, is 2210 amps for s = -0.8, giving an ohmic loss for both sides of 465 watts which is limited by the skin depth of the copper. The ratio of this ohmic loss to that in the fluid, neglecting the profile factor, is 0.163 for this generator independent of the slip, so that the power density in the generator will be decreased. This is an upper limit, in practice the fluid current constraints should reduce substantially the ohmic loss in the copper.

2.2.2 Traveling-Field Structure

The purpose of the traveling-field structure or stator is to produce the required magnetic field with the minimum of distortion from a pure traveling sinusoid. The effect of distortion is to generate spatial harmonics with a shorter wavelength and slower field velocity, and consequently to reduce the efficiency due to the increased ohmic losses in the fluid. Distortion is created by many sources, the most important being the slots in the iron structure for the winding, the use of a finite and small number of phases with pulsed rather than sinusoidal turns densities, and saturation of the iron. To minimize these effects, the following design ideas were adopted:

1. The two stator cores were designed so that they can be operated with tooth opposite tooth or with tooth opposite slot in order to reduce slot harmonic effects and study them experimentally. This is accomplished by making the two end teeth of different widths so that reversing one core relative to the other switches cases. The core lamination dimensions are shown in Fig. 3, and the experimental fields produced by the two cases are compared in Section 3.1. Also, short straight sections are provided at the end of each slot to allow the later insertion of highly-permeable slot plugs which would smooth out the air-gap magnetic field at the price of increased leakage flux.

2. More than one slot per phase per pole or else more than three phases, either of which requires more slots per wavelength, were used, and this results in a smoother field as explained previously [18].

3. Instead of using a rectangular slot, the width of the slot (or tooth) was tapered so that more iron area is available where needed to handle the leakage flux without saturation.

The traveling-field-structure design results are only summarized here, as they are presented in detail in Reference 18. In the experimental generator there was only room for 12 slots. The number of ampere turns was calculated to be 1230 per slot at s = -0.8, the maximum case, including the Carter coefficient and a small allowance for iron reluctance. Each coil consists of 45 turns made out of three #14 wires in parallel in the slot butt-soldered to a rectangular bar of about twice the copper area outside the slot. The coil loss was estimated to be 440 watts for this case using an assumed effective copper area of 0.7 and a larger copper area outside of the slot. (This is low because the effective area was off, and will be increased to about 700 watts.) The core loss for the Armco electrical steel M-14 was estimated to be 92 watts including the lamination packing factor. A core section with a partial winding is shown in Fig. 4. One completed coil is visible showing the joints

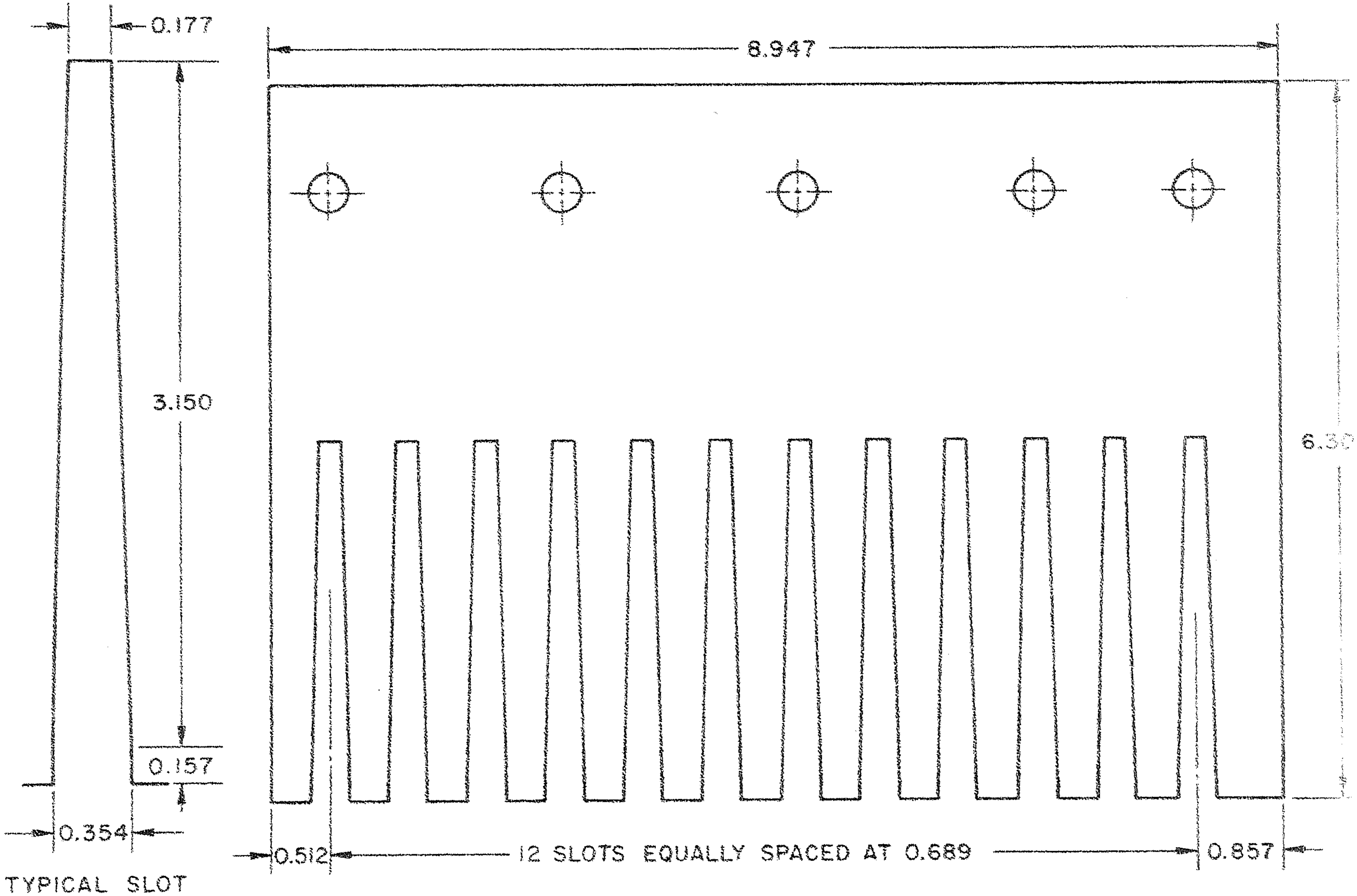

Fig.3 Traveling-field-structure lamination

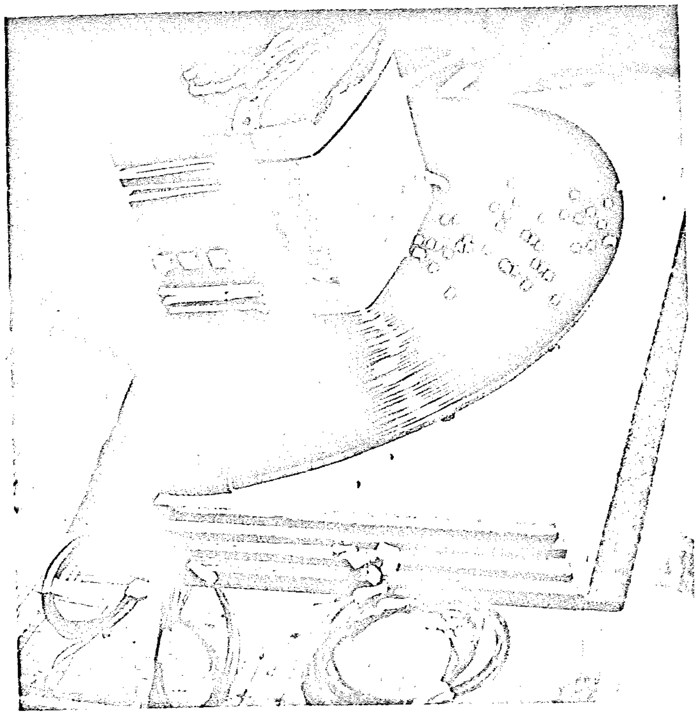

Fig. 4. Core section with partial winding.

Fig. 5. Completed core section.

between the two wire sizes (covered with insulating sleeves) and some of the pick-up coils used to monitor the field. The completed coil structure is shown in Fig. 5.

One important point in the stator design is to build in adequate monitoring devices. Two types are required - thermocouples to measure the coil temperatures because of the danger of overheating at high magnetic fields and the thermal effect on ohmic losses, and small pick-up coils both at various locations in the slots and also in the loop around the back of the core. There are 19 two-turn magnetic-field monitoring coils on each core, located as shown in Fig. 6. The locations were chosen to observe the field in the core above the slots, which includes the compensating flux (see the next section); the flux through some of the teeth, including the leakage flux; the flux through some of the slots; and the flux entering the air gap. They will be useful in evaluating the stator design and in monitoring the operation with fluid present in the channel since the field cannot be directly measured.

2.2.3 Compensating Poles

In the regions where the fluid enters and leaves the traveling magnetic field undesired voltages and currents are induced in the fluid, and these cause increased ohmic losses. In order to set up the proper boundary conditions so that the traveling-field region acts like a segment out of an infinitely-long machine, Elliott proposed the use of compensating poles [21]. The peak magnetic flux density B_c and length L_c must satisfy $B_c L_c = B\lambda/2\pi$ assuming a slit-channel machine. Arbitrarily choosing L_c to be one inch gives $B_c = 0.525$ wb/m The channel wall thickness under the compensating poles was increased to 1/8-inch to give a stronger structure because the poles are removable. Then, 2380 ampere turns is required for each of the four pole structures, and 85 turns with a tap at 70 turns are on each pole. Excitation is by means of the phase voltages rather than the phase currents because this tends to be self-compensating for the phase shift required as the fluid reaction field varies. (This is discussed in Reference 18.)

Insulating vanes in the channel under the compensating poles are required to reduce the ohmic loss, but at the penalty of increased viscous loss. It is necessary to calculate (or estimate) both losses as a function of the number of vanes and optimize. The viscous loss is easily calculated using the available hydrodynamic equations, but the ohmic loss can only be crudely estimated. Using the results of Moszynski [22] to estimate the ohmic loss, a compromise of six vanes was selected.

2.2.4 Discussion

The results of the previous calculations are summarized in Table III to give a tentative idea of the performance to be expected from the experimental generator at three values of slip. All of the losses are considered, except that the field harmonics are not included and perfect end compensation is assumed. The effect of the copper side bars is to reduce the fluid current and

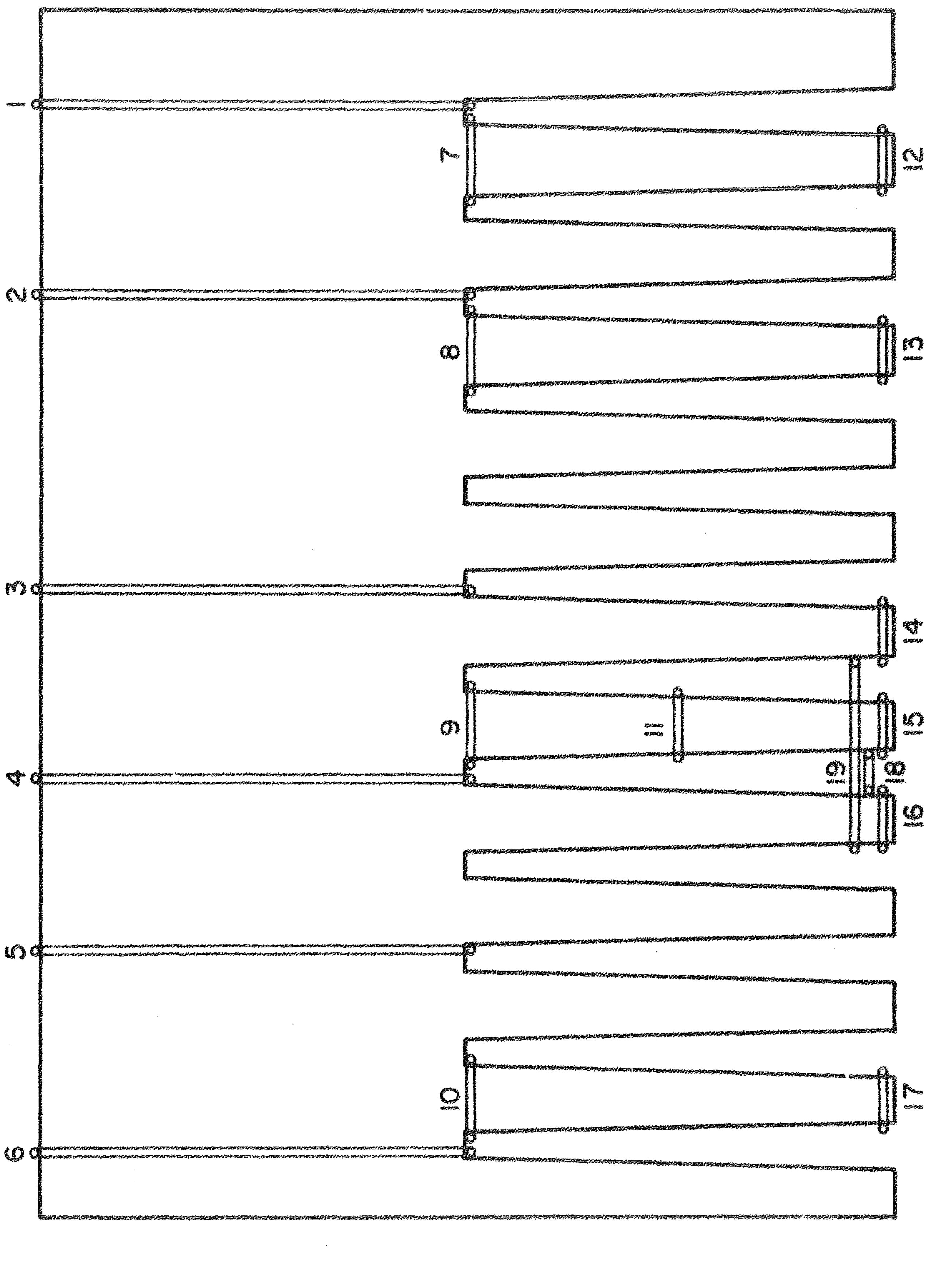

Fig. 6. Magnetic-field monitoring coil locations

Table III. Summary of theoretical generator performance.

Parameters	Units			
s		-0.8	-0.5	-0.3
$(\frac{1}{1+\beta})P_s$	watts	3070	1920	1150
P_e	watts	640	590	560
P_{core}	watts	90	90	90
P_{cp}	watts	230	230	230
P_{out}	watts	2110	1010	270
$\frac{p'_m}{P_s}$		1.67	1.42	1.26
P'_m	watts	5980	3160	1680
Δp_{em}	psi	55.0	34.8	21.4
Δp_v	psi	9.4	6.8	5.2
Δp_{cp}	psi	10.8	7.5	5.6
Δp_{tot}	psi	75.2	49.1	32.2
P_{in}	watts	8190	4460	2530
e_g		0.26	0.23	0.11

thus the power density. This effect is estimated by assuming that the induced electric field or voltage in the fluid stays constant since the magnetic flux density is assumed to be constant. (This means that the sum of the ohmic losses in the fluid plus the side bars decreases as the bar conductivity decreases.) The ratio of the ohmic loss in the side bars to that in the fluid neglecting the velocity profile correction is defined as β, where β = 0.163 for this generator from Section 2.2.1. Then the ratio of the equivalent resistances of the two regions is also β, and the fluid current is multiplied by $1/(1+\beta)$ for the same induced voltage. Finally, the generated power in the fluid, which depends on $E \cdot J$, is $P_s/(1+\beta)$; where P_s is the power without the side bar correction, Table I. The mechanical input power modified for the side bar correction is P_m.

The separate power losses are also included in Table III. The ohmic loss in the exciting winding is based on the measured DC coil resistances. The reduction in the fluid currents due to the bars also appears here because the reaction field and thus the required ampere turns are reduced. This is taken into account by multiplying sR_{Mf} by $1/(1 + \beta)$, and amounts to decreases in excitation loss of 15%, 8%, and 3% for s = -0.8, -0.5, and -0.3. The core loss, P_{core}, is essentially independent of slip or the side bar effect except for the slight change in the leakage flux which is ignored. The excitation power for the compensating poles, P_{cp}, depends only on the flux density which is independent of the slip. The net electrical output power is P_{out}.

Similarly, the mechanical pressure drops are taken from the previous results. The electromagnetic term Δp_{em} comes from P_m', and Δp_v is given in Table I. The pressure drop for the compensating poles, Δp_{cp}, is estimated by assuming that the electrical drop is equal to the viscous drop since the calculation for the electrical pressure difference was very rough. The net result is estimated efficiencies of 0.26 at s = -0.8, 0.23, at -0.5, and 0.11 at -0.3.

2.3 THE FLOW LOOP AND INSTRUMENTATION

The existing NaK-N_2 flow loop at the Argonne National Laboratory with the addition of a new extension intended specifically for the induction generator is used for these experiments. The purpose of the flow loop is to supply the required NaK and nitrogen flows in an easily controlled and measured fashion for the tests. The existing loop is shown in Fig. 7 and the extension, which is connected to the two flanges on the left side of the existing loop, is shown in Fig. 8. After descriptions of the loop and extension, the control systems for the NaK and nitrogen flows and the instrumentation are discussed.

The pump, heat exchanger, supply tank, separation system, and part of the control system are utilized from the existing loop. The flow path is from the supply tank to the pump, then through the heat exchanger and out of the top left flange to the extension and the generator. The flow returns to the storage tank through the bottom left flange. (The valve in the vertical section between the two flanges is closed.) For the two-phase experiments the supply tank also serves as the separator, with the nitrogen flowing through the two small pipes from the supply tank to the separation tank and then out to the atmosphere.

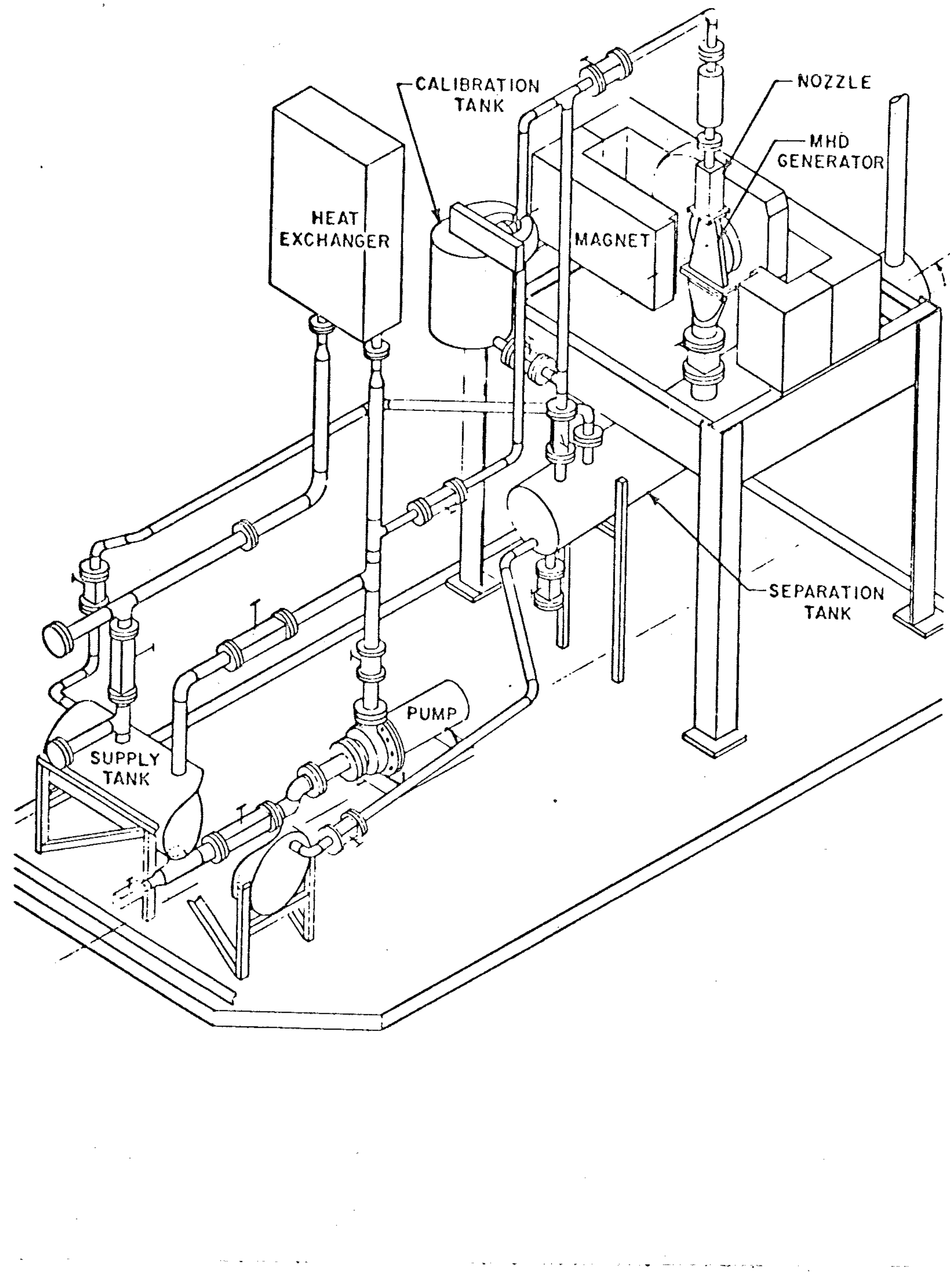

Fig. 7. Schematic of NaK-N_2 loop.

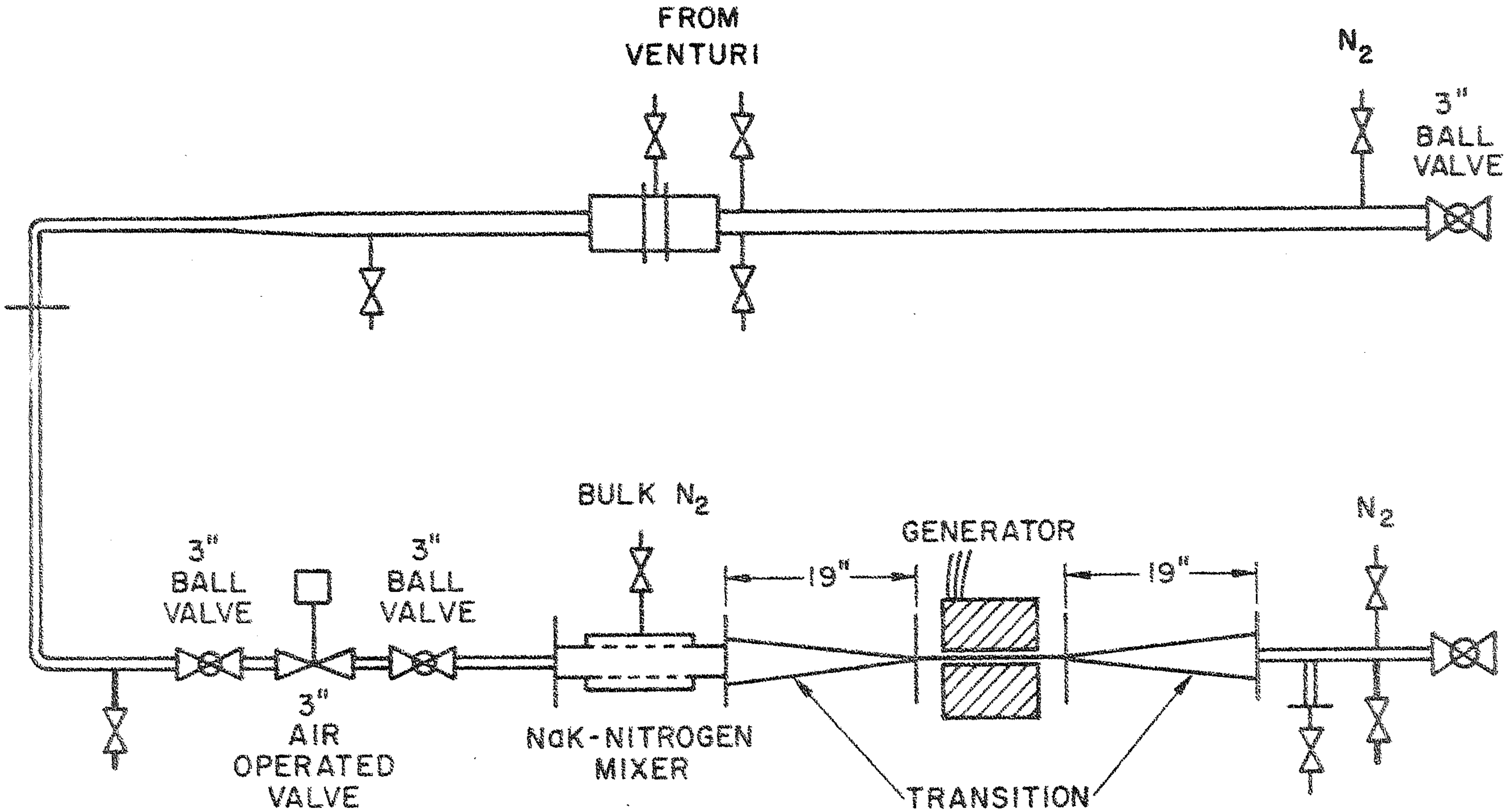

Fig. 8. Addition to loop for induction generator tests.

Two pumps of different capacity are available, and may be used individually or in series. Both are of the same type and feature a combined rotor-impeller assembly with a completely sealed or canned stator winding. A small portion of the pumped NaK is allowed to recirculate through the rotor cavity to cool the motor and also to lubricate the aluminum oxide bearings. This construction leads to a compact pump with no possibility of leakage, but since it dumps nearly all of the motor ohmic loss into the NaK it may also cause an excessive temperature rise in the NaK flow. The small pump has a 25 gpm capacity at 150 ft. head, and the large pump has a 250 gpm capacity at 220 ft. head. Only the large pump will be used here because of the required flow capacity.

To maintain the NaK temperature below about 125°F, required for the fiberglass test section, a stainless-steel finned-tube NaK-to-air heat exchanger is used. Although in the pump bypass loop for the DC generator experiments, the heat exchanger is in series with the extension, and this is most convenient here as both the full pump output and the maximum cooling are required. The cooling capacity of the heat exchanger is approximately 12 kilowatts at an outside air temperature of 75°F, a NaK inlet temperature of 150°F, and a flow rate of 100 gpm; but this is less than the power dumped into the NaK by the pump.

The extension for the induction generator tests, Fig. 8, is a U-shaped section about 12 feet long containing a venturi for measuring the NaK flow rate, a three-inch air-operated valve to control the pressure across the test section, and three-inch ball valves to isolate the extension from the rest of the loop and from the test region so that changes can be easily made. The test region includes the mixer for adding nitrogen to the NaK flow, the fiberglass test section, and a T-section so that the spare pump and a cyclone separator may be added for later tests at very high void fractions.

The NaK flow through the test section is controlled by means of the air-operated shunt or bypass valve between the pump and the supply tank in the existing loop and the air-operated series valve in the extension because constraints on both the volume flow rate and the pressure difference are required. The pump operates at (approximately) fixed speed so that a single valve is not adequate. The NaK volume flow rate is measured by means of the venturi in the extension coupled with a differential pressure transducer.

The nitrogen supply for the experiments will be obtained from a 42,500 ft^3 capacity trailer. The nitrogen is fed into the mixer through four check valves to prevent flow of the NaK back into the nitrogen system. The mixer consists of an 11-inch length of three-inch Schedule 10S stainless steel pipe with 900 1/8-inch diameter holes enclosed by a concentric length of five-inch Schedule 40 pipe into which the nitrogen is introduced. The nitrogen flow will be measured with an orifice and a differential pressure transducer. It will also be necessary to measure the void fraction by means of a gamma-ray source and a scintillation photo-multiplier tube.

Pressure measurements in the test section are made by means of gauge-diaphragm seal assemblies. A 316 stainless steel diaphragm is welded to the upper chamber in a two-chamber, 316 stainless steel pot assembly. The upper chamber is connected to a gauge and/or a transducer by tubing and the upper assembly is filled with instrument oil. The gauge accuracy is 1/2% of full scale. The lower chamber of the diaphragm unit is connected to the test section and to a bleed system for purging. Five pressure taps are provided on one side of the channel with a spare set on the other side. The tap locations are at the entrance, exit, and center of the traveling-field region and the outer ends of the compensating poles.

The experimental generator in place in the flow loop is shown in Fig. 9. The vertical bolts and the I-beams above and below the magnet cores are the mechanical support system. Also shown are the support systems for the compensating poles (replaced here by micarta blocks) and the copper side bars. The vertical I-beams maintain the vertical alignment of the generator components. The generator is enclosed by an aluminum and lucite box during operation, part of which is visible.

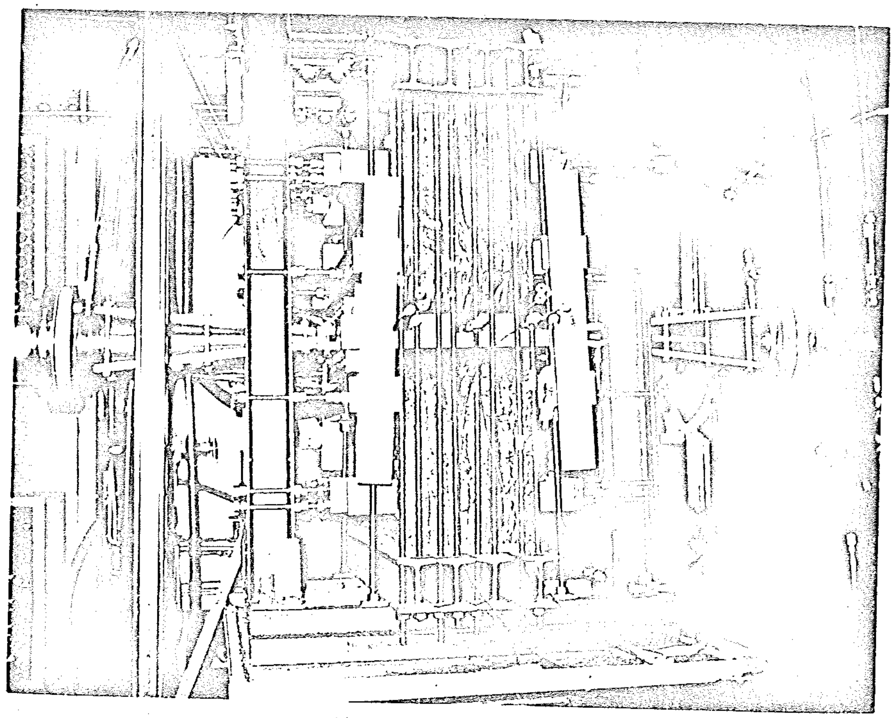

Front view.

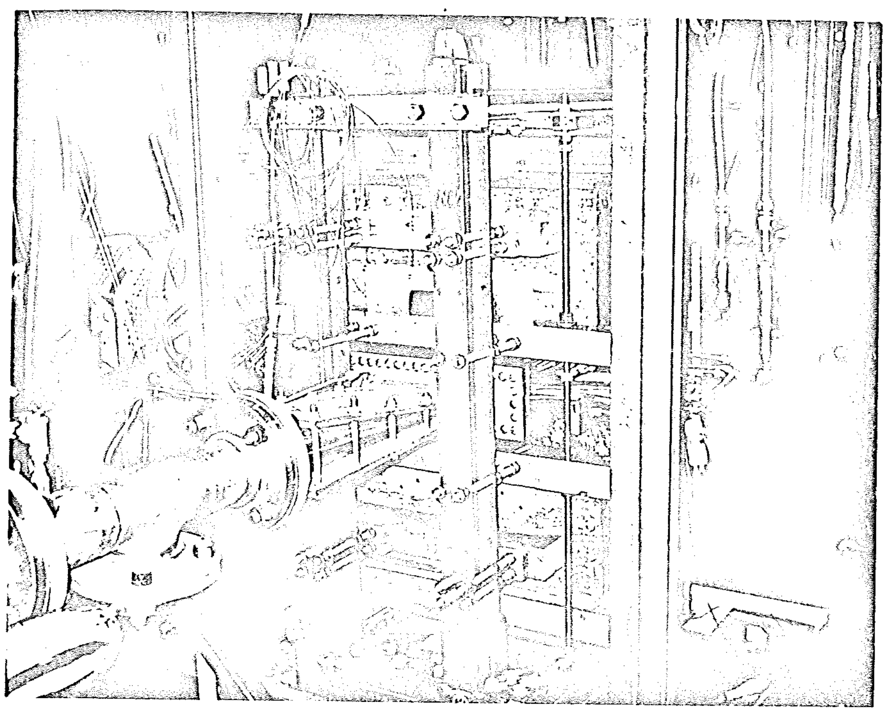

Side view.

Fig. 9. Two views of the generator installed in the flow loop.

SECTION III

EXPERIMENTAL RESULTS

3.1 PRELIMINARY FIELD TESTS

The purpose of the preliminary field tests with no fluid or fluid channel was to check the operation of the electrical system - both control and measurement, to determine the magnetic field produced by the traveling-field structure, and to determine the magnetic field produced by the addition of the compensating poles. At the same time the electrical loss in the stator and the operation of the magnetic field monitoring coils were studied. Problems in the experimental electrical system were determined and corrected so that satisfactory operation could be attained.

The original excitation system for the generator consisted of a three-phase delta-connected electrical source driving the wye-connected generator through three single-phase wye-connected variable autotransformers. Under the unbalanced load conditions represented by the open magnetic circuit of the generator and the compensating poles, it was not possible to properly control the phase or coil voltages and currents as they interacted through the floating neutral. Thus the excitation was changed by transformers to a wye connection, constraining the phase-voltage phase angles to be within about one degree of $\pm 120^{\circ}$. The wye connection of the generator was preserved because it allows easy control of the phase voltage or current magnitudes with the variable autotransformers. Test results for this case showed that the current phase angles still varied greatly from $\pm 120^{\circ}$. Since the currents produce the magnetic field, their correct phase angles are crucial to the production of the desired magnetic field. The generator was modified by the use of a symmetrical connection of the coils, with the coil at each end and the two central coils from each stator connected to the same phase. This resulted in better phase relations for the currents. (Excitation currents of arbitrary phase angles can be treated by known methods [9]).

The equivalent-circuit terminal parameters of the generator were measured. The dc phase resistances, measured with a Kelvin bridge, were 0.1918 ohms, 0.1929 ohms, and 0.1919 ohms. The ac parameters were measured at a frequency of 1000 hertz with an impedance bridge. With the other phases open the inductances were 10.0, 12.45, and 12.46 millihenrys; and the Q's were 20.8, 24, and 23.2. With the other phases shorted the corresponding values were 7.11, 7.71, and 7.75 millihenrys; and Q's of 13.8, 13.3, and 12.6.

The objective of further field tests, in addition to those already reported [18,23], was to check the new excitation method and to measure the resulting magnetic field and terminal properties. The magnetic field for the symmetrical wye-connected excitation is shown in Fig. 10 for an excitation current of 40 amps per phase. For this case the current phase angles were $+129.8^{\circ}$ and -127.3°, and the total power dissipated in the magnet structure was 1340 watts. The three phases are still unbalanced, with phase current to voltage angles of

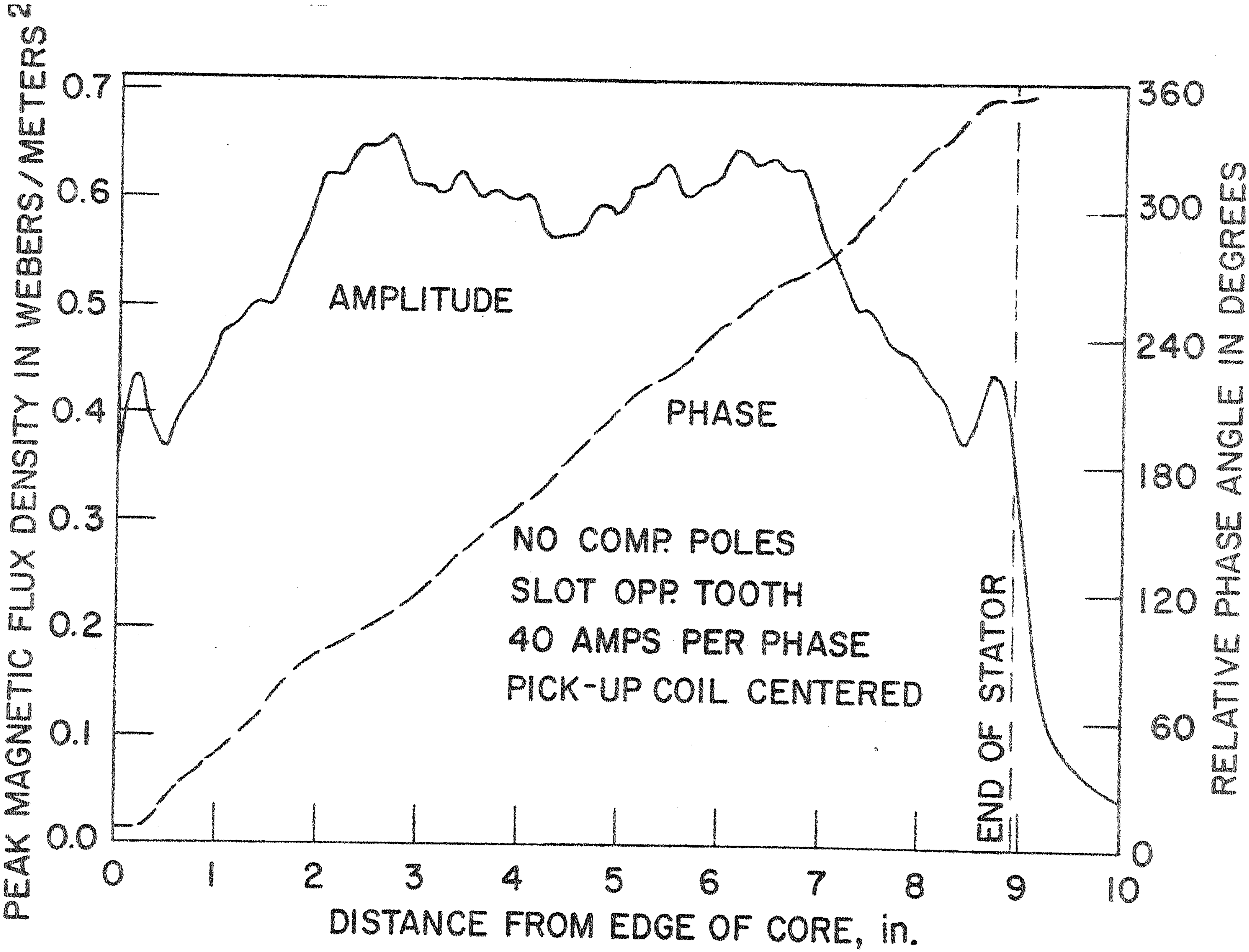

Fig. 10. Magnetic field amplitude and phase with symmetrical wye-connected excitation.

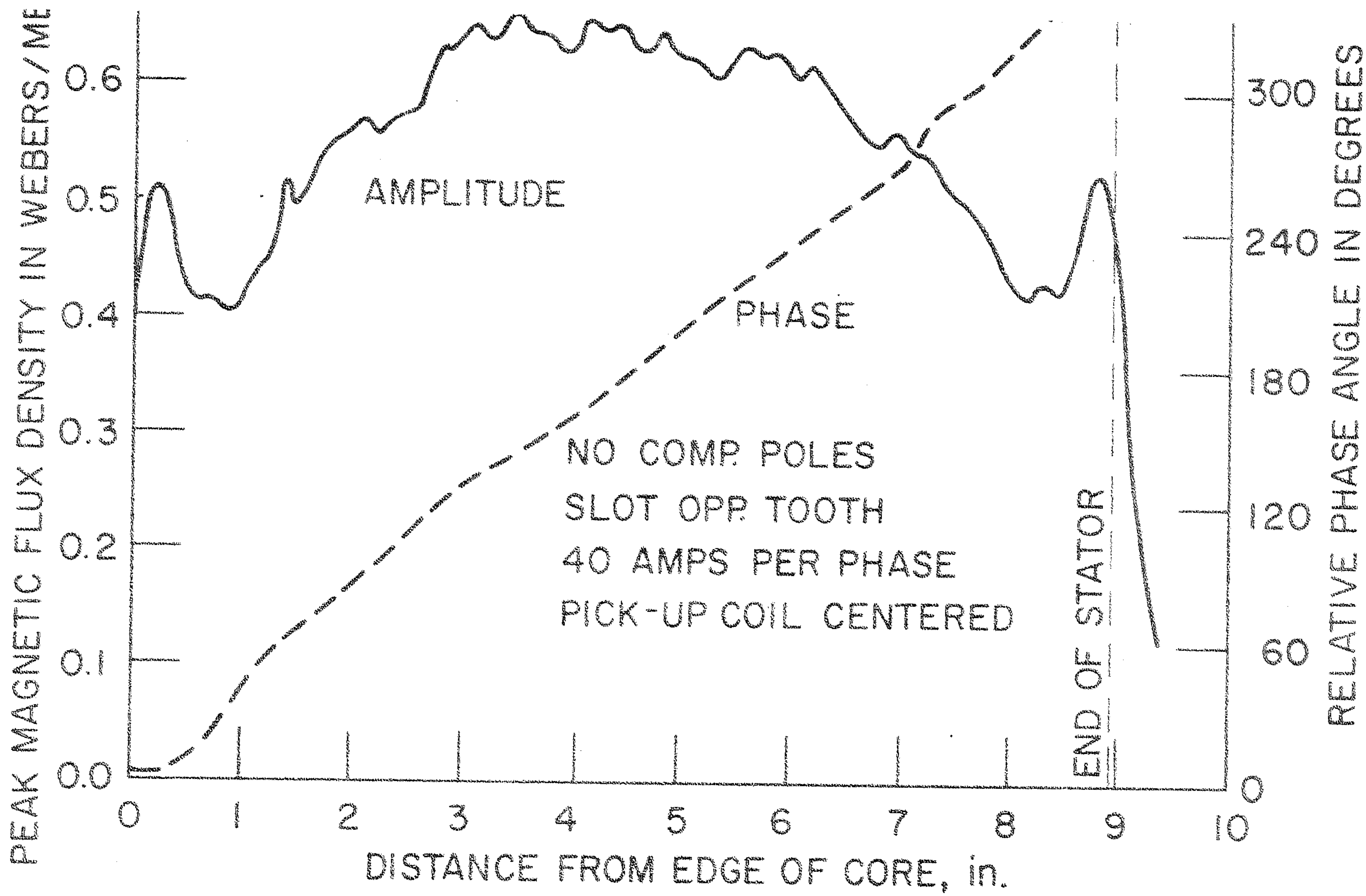

Fig. 11. Magnetic field amplitude and phase, original excitation

87.6°, 97.0°, and 79.3° respectively. The qualitative shape of the magnetic field, both magnitude and phase, is quite similar to the previous results [18,23], except for a slightly smoother field in the center of the traveling-field region. For comparison, the magnetic field at 40 amps per phase for the original excitation is shown in Fig. 11.

For the field tests and the generator tests the phase or line currents were set (except for the self-excited cases) as they control the magnetic field, and the other quantities were measured. All current measurements utilized Weston Model 461 current transformers with Weston Model 370 ammeters. For the line-to-neutral and line-to-line voltages both a Weston Model 904 voltmeter and a Non-Linear Systems Model X-2 digital voltmeter were used. The powers were measured by means of low-power-factor Weston Model 432 wattmeters, 0.2 pf full scale at rated voltage and current. The phase-angle measurements used a Wiltron Model 351 phase meter coupled to a digital voltmeter. The current input signals for the phase meter were taken from 0.1 ohm straight nichrome strips in the secondary of the current transformers, and the voltage input signals from dropping resistances to approximately equalize the magniturdes of the various input signals. The magnetic field profiles were measured by means of a 1/4-inch diameter, twenty-turn pick-up coil mounted on a ruler. Measurements were made at 1/16-inch intervals. The digital voltmeter and phase meter were also used to measure the signals from the pick-up coils and the magnetic-field monitoring coils.

For some of the flow tests the coils in the slot at either end of the stators were shorted to reduce the fringing field through the end teeth. The magnetic field and terminal properties without the fluid present were not measured for this case.

The support system for the magnet, visible in Fig. 9, although located outside of the main field region, contains a considerable amount of metal. The influence of the support system on the magnetic field in the channel was checked and found to be negliginle. The ohmic loss in the support structure at 40 amps per phase is less than the ± 100 watt fluctuation in the total power loss due to changes in magnet temperature and inaccuracies in setting the currents. The influence of the stainless steel transition pieces and flanges was also checked by inserting them into position. With the compensating poles removed there was no measurable change in the terminal properties.

The fiberglass channel has copper side bars, as shown in Fig. 1 to short out the fluid currents and reduce the effects of finite width. The copper bars are inserted into the channel to support the field structures, and are locked against the edge of the core by external supports so that motion during operation is not possible. The empty-channel tests were limited due to the rapid heating of the copper, but the added loss amounted to 500 watts at 25 amps per phase and 1180 watts at 40 amps per phase. This is comparable to the ohmic loss in the copper expected due to the fluid currents. Of course, the current patterns will be different with the fluid present. The monitoring-coil and terminal voltages were both reduced by about 6 per cent with the copper present, indicating a corresponding change in the magnetic field.

3.2 ZERO-FIELD FLOW MEASUREMENTS

The zero-field flow measurements are used to establish the flow conditions in the generator channel, and to check out the flow system and instrumentation. The volume flow rate is measured by a venturi and differential pressure transducer, and the pressures by gauges. The instruments are isolated from the NaK by stainless steel diaphragm seal assemblies. Flows of up to 285 gpm or 83.9 ft/sec were obtained, slightly about the design value of 250 gpm. Higher flows were possible but were not attempted to avoid possible damage to the system, and because the higher velocities could not be obtained with the magnetic field excited.

Examination of the measured pressure gradients showed that they were between two and three times the theoretical values. Significantly, the pressure gradient along the channel increased as the static pressure decreased. These point toward gas mixed with the liquid due to the high flow rate from the supply tank. Additional NaK was added to the loop. The pressure gradients then decreased significantly, but they still ranged up to two times the theoretical values. Typical values before and after adding NaK are shown in Table 4.

TABLE 4. Zero-field flow data.

Fluid velocity ft/sec	Pressure gradient, Measured	psi/inch Calculated
After adding NaK		
28.2	0.32	0.20
33.2	0.41	0.27
40.8	0.65	0.38
60.2	1.40	0.77
79.9	2.66	1.29
Before adding NaK		
28.0	0.45	0.19
33.5	0.60	0.27
40.7	1.05	0.38
62.9	1.90	0.83

More tests, by adding still more NaK, showed that no further decrease in the pressure gradient occurred. The pressure gradients are above the theoretical value, and this is probably due to channel roughness. Recent measurements of the pressure gradient covering the full range of fluid velocity are shown in Fig. 12, along with a few of the early points.

3.3 GENERATOR TESTS

The many series of generator tests are divided into five groups. First, operation from the 60-hertz power line is covered, including both generator and pump cases. Second, some results with the coil at each end of both stators shorted are presented, again covering both generator and pump operation. Next, self-excited operation is discussed. Fourth, some harmonic measurement results are presented as they may be important for system operation. Finally, some miscellaneous cases are covered. Only data with the unvaned channel is presented

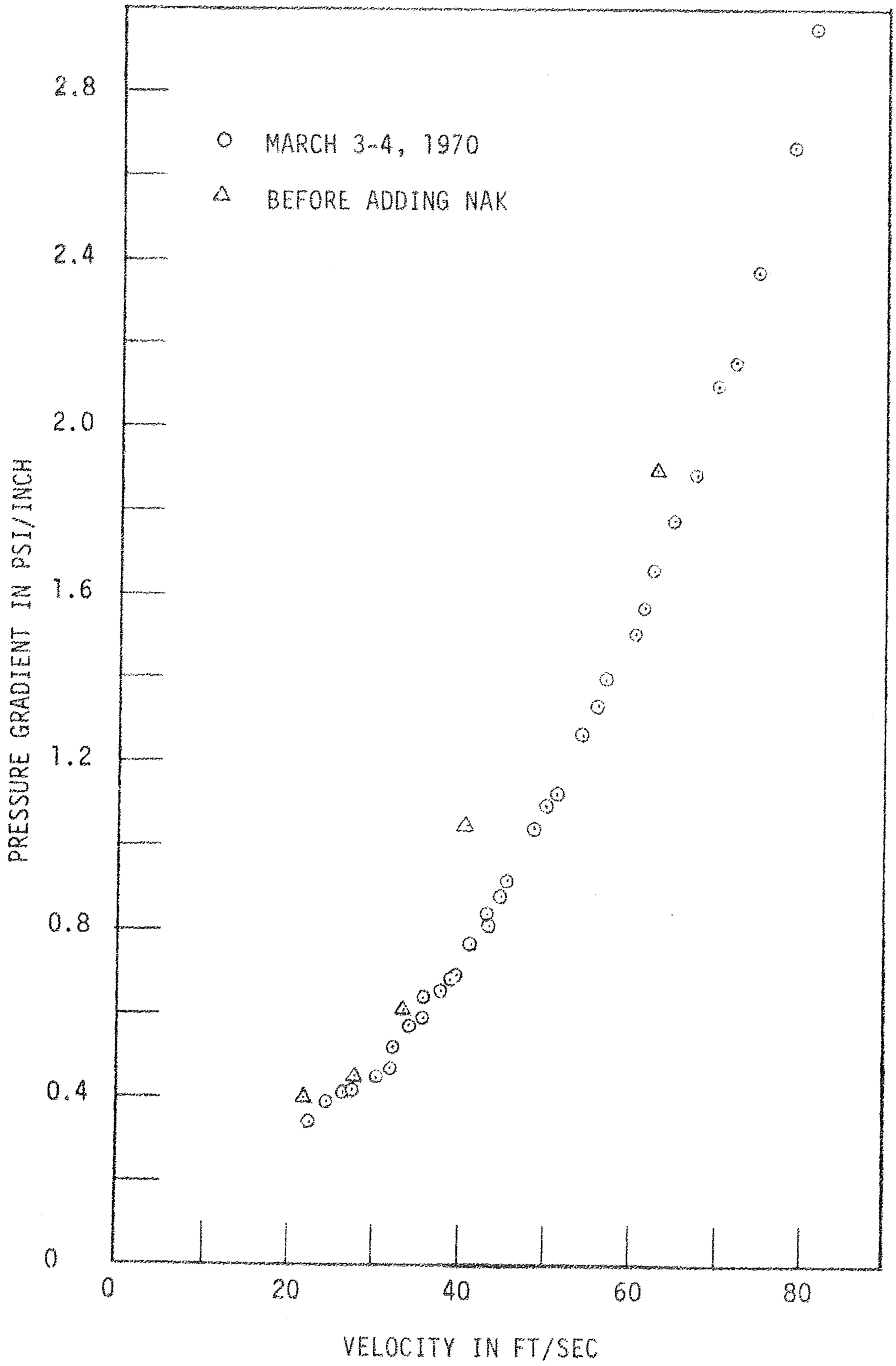

Fig. 12. Zero-field pressure gradients.

because the vaned channel was warped so that the leaks could not be eliminated.

A kerosene cooling system for the electrodes was installed to eliminate the possibility of damage to the channel due to electrode overheating. The copper cooling coils are visible on top of the copper electrodes in the photograph of the channel, Fig. 2. During the early data runs, currents of at least 75 amps through the cooling system between the electrodes were measured at 25 amps per phase. This current is small compared to the about 2000 amps peak expected in the electrodes, but could influence the end loss. Insulating connections were installed in the cooling system to eliminate the currents, and the electrode voltage difference was monitored. The electrodes are in direct contact with the iron core, but the lamination insulation is sufficient to make currents through the core megligible.

3.3.1. Normal Operation from Line

Data points were measured for various terminal conditions and excitation currents between 20 and 40 amps per phase. Attention is confined here primarily to the results for 20 amps per phase because with the reduced electromagnetic pressure gradient higher fluid velocities could be attained. Pump operation at higher currents was also limited due to excessive vibration and/or cavitation. The power and efficiency are increased for higher excitation currents, but the qualitative behavior is the same.

The net power input is plotted as a function of the fluid velocity in Fig. 13 for some of the early data points,with negative numbers corresponding to power output. The synchronous velocity v_s is 41.3 ft/sec. The data points fall into three distinct groups, each with its own slope. The largest group corresponds to normal excitation points measured before the addition of more NaK to the system. The second group, measured after the addition of NaK, has an almost identical slope with a shift toward higher velocity of about 4 ft/sec. This agrees with the two-phase hypothesis discussed in Section 3.2 because at the (supposed) higher quality (more gas) of the first group, the actual velocity in the generator channel would be higher than that measured at the venturi because of the lower channel pressure. The third group, with the end coils shorted to reduce fringing of the magnetic field, was measured after the addition of more NaK. (This case is treated in Section 3.3.2.)

The powers for the 46 data points measured at 20 amps per phase after eliminating the two-phase problem are shown in Fig. 14. There is relatively little scatter, the operation of the induction generator (pump) and flow system was very stable and repeatable, and operation for up to eight hours per day was easily obtained. Note that the net power did go negative, corresponding to generator operation, but the power flow was not balanced between the phases. (Power always flowed into one phase.) This in itself is significant because it was not clear if net generator operation could be obtained with a one-wavelength generator with no end compensation.

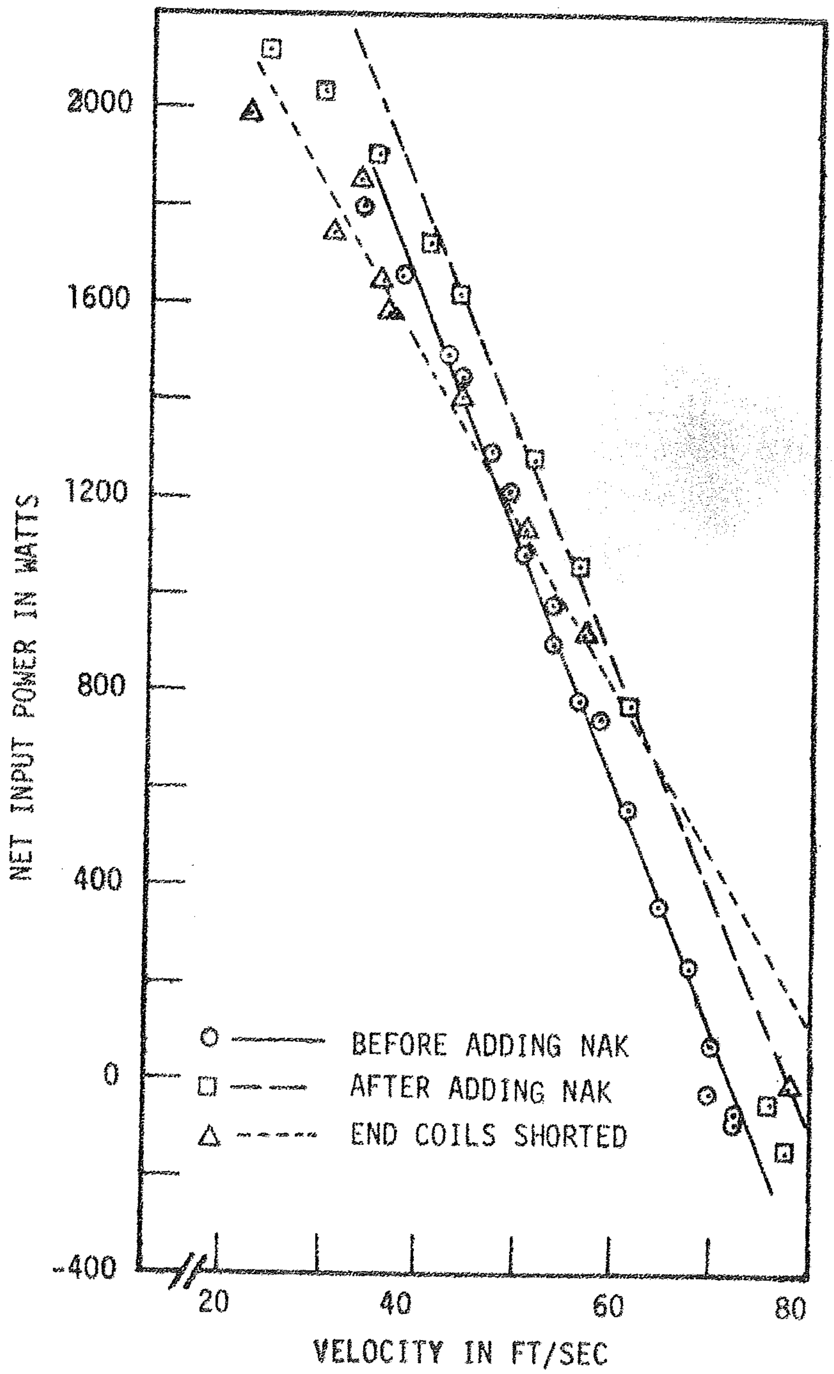

Fig. 13. Net Input power versus fluid velocity, early data

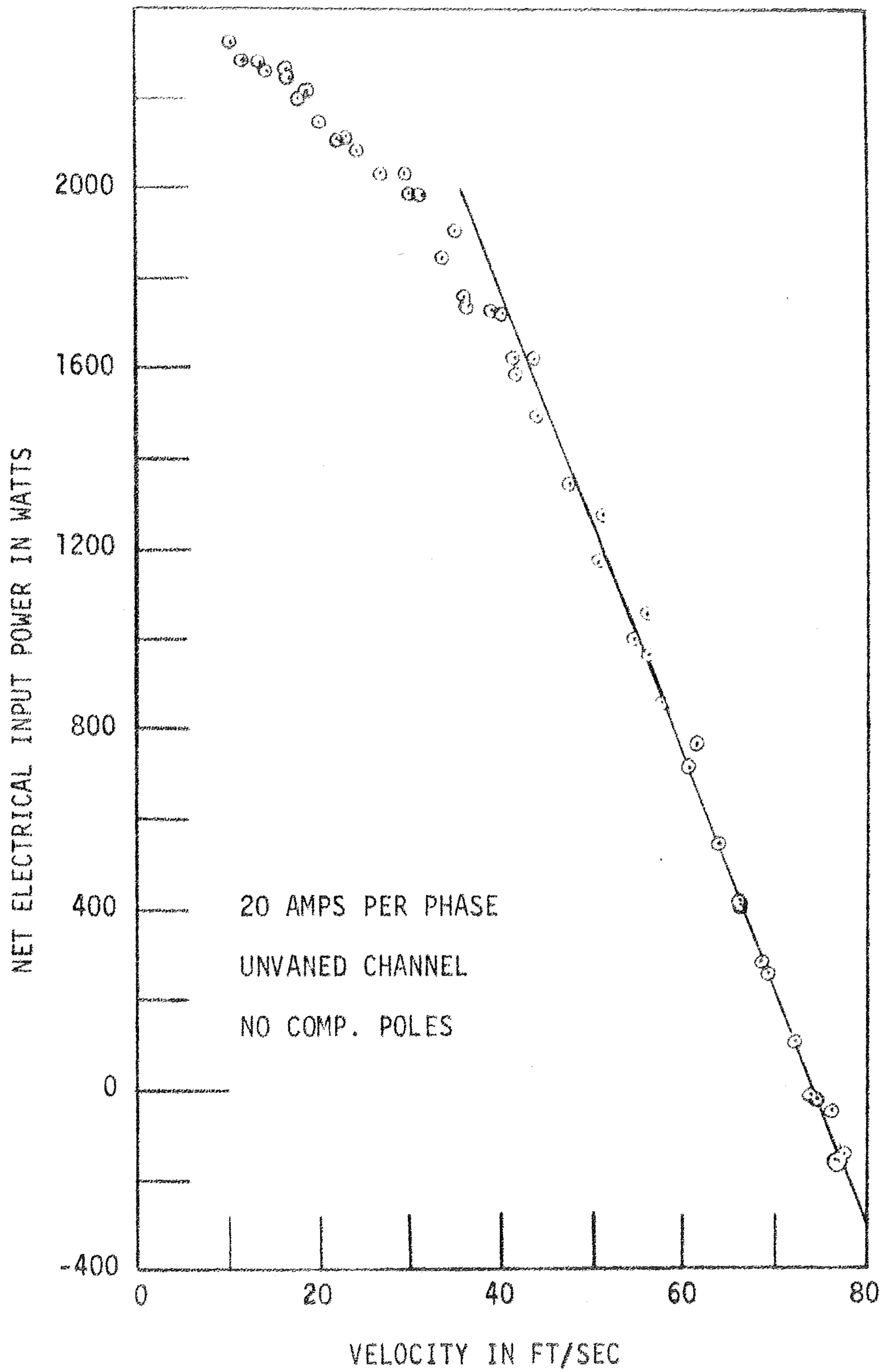

Fig. 14. Net input power versus fluid velocity, later data

At zero slip, 41.3 ft/sec, there is a significant power loss. Much of this is expected as coil loss, but there are other significant contributions - probably due to the copper side bars, ends, fluid velocity profile, and poor current phase angles (around 10° off from ±120°).

One 40-amp point is shown on Fig. 14, with the power divided by four to account for the differences. This is the square point shown at 400 watts. The 40-amp point fits so closely with the 20-amp points that saturation cannot be significant up to this magnetic field strength.

The voltage from monitoring coil 14 on the upper core (see Fig. 6) is plotted as a function of the fluid velocity in Fig. 15. This coil was chosen as a good measure of the magnetic field strength in the channel. For constant-current excitation the magnetic field should vary as $1/(1 + s^2 R_M^2)$. Again the points fall into the same three distinct groups as with Fig. 13.

The voltage difference between the two copper electrodes as a function of the fluid velocity is shown in Fig. 16 for the data points with the end coils excited. The voltage is normalized by dividing by the upper monitoring coil 14 voltage to eliminate the effect of variations in the magnetic field. Here also two distinct groups are seen with the same separation of about 4 ft/sec. With proper compensation for the ends the electrode voltage difference should be zero.

3.3.2 End Coils Shorted

The end coils on each stator were shorted to reduce the fringing magnetic field, or in a sense to allow the generator to provide its own compensation. The first few points measured for this case are shown in Fig. 13, and the complete set of 26 points in Fig. 17.

This case does not appear attractive because the slope of the power versus velocity curve is reduced from that for the previous case, or there is less useable power. This case was also run in the self-excited mode, but the power outputs were again reduced from the normal case.

3.3.3 Self-Excited Operation

By connecting capacitors across the terminals of the induction generator to supply the required reactive power it is possible to make the generator run in the self-excited mode - without any connection to the power line. The generator operates as an oscillator producing net power output, with the resonance occuring between the inductance of the generator and the external capacitance. The main points noted during the tests were:

1. Operation is very stable, and there is no trouble with fluctuations.

2. The generator will start itself with no external trigger required. All that is needed is to bring the fluid up to a high-enough velocity (with adequate pressure available) and connect sufficient capacitance

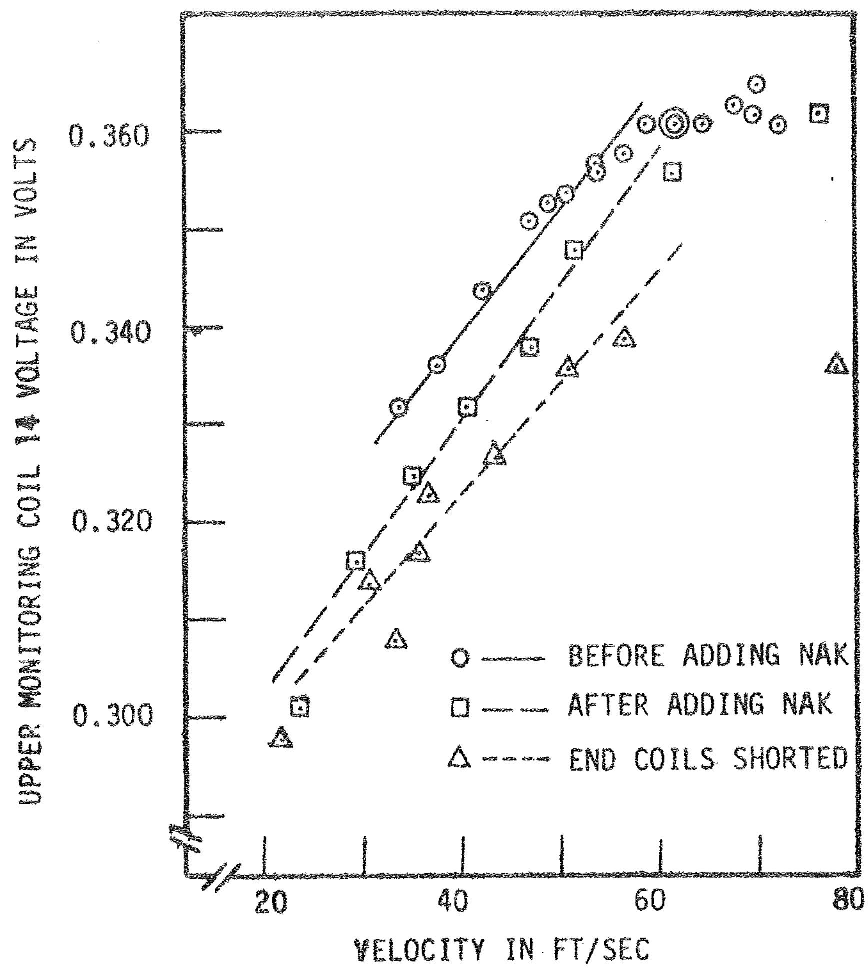

Fig. 15. Upper monitoring coil 14 voltage versus fluid velocity.

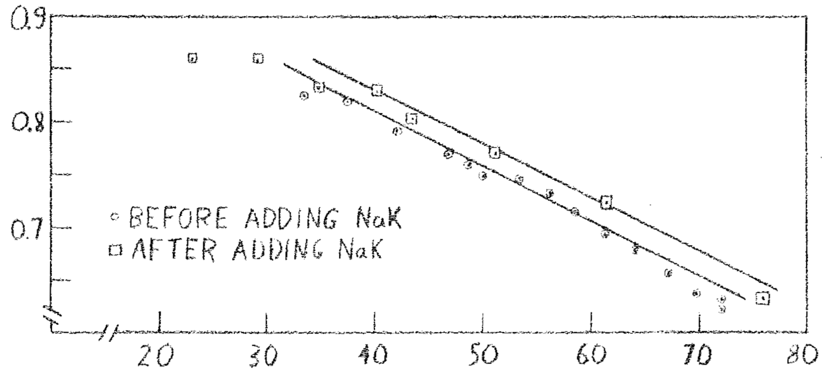

Fig. 16. Normalized electrode voltage difference versus fluid velocity.

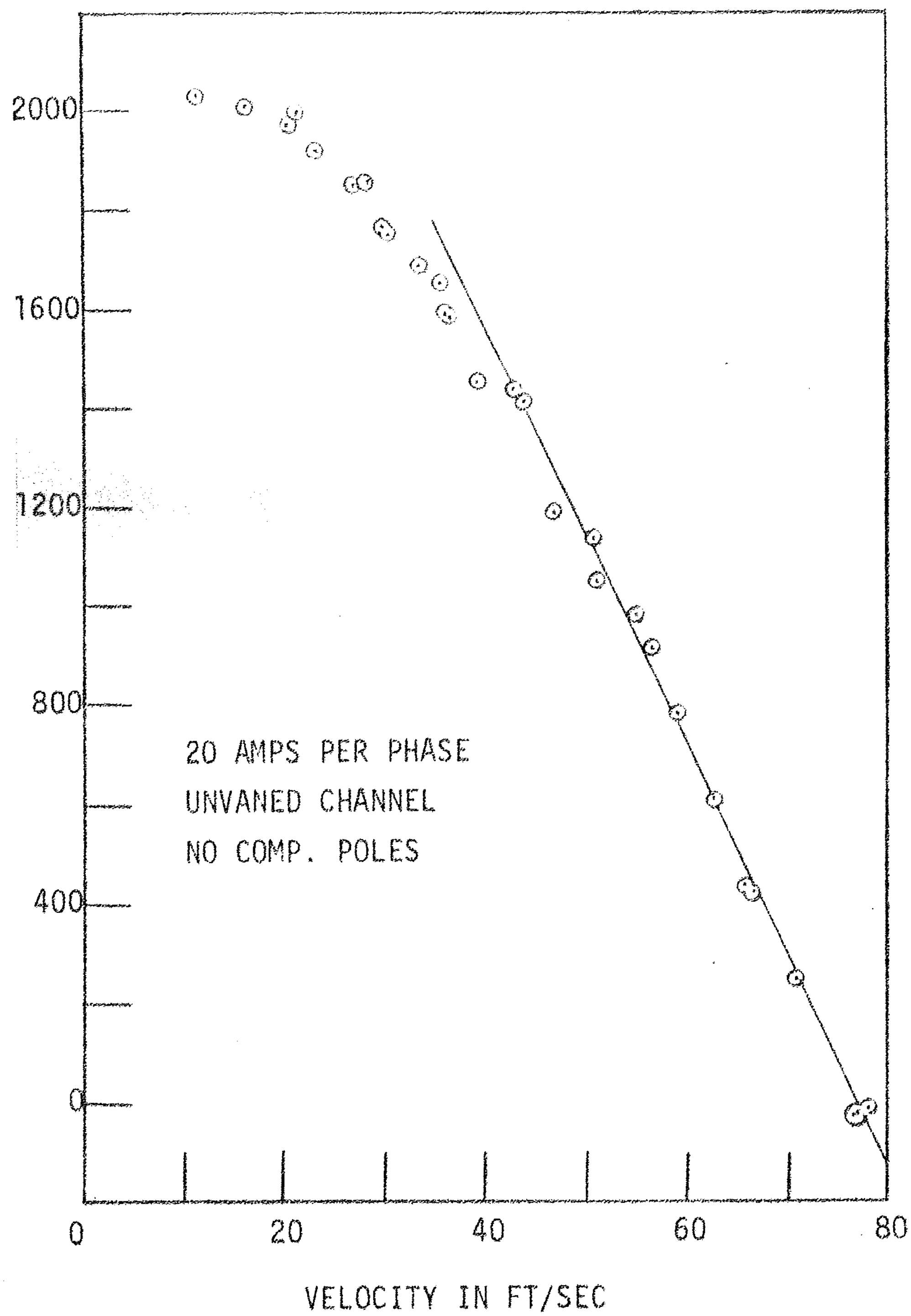

Fig. 17. Net input power versus fluid velocity with end coils shortened

across the terminals, and the generator will start. The generator will start either without or with a resistive load, but it can carry a heavier load than it can start with.

3. The frequency is controlled by the external capacitance, and can be varied at will provided only that the fluid velocity is enough above the synchronous velocity at that frequency to supply the required power. The change in frequency from no load to full load at a given capacitance value is only a few tenths of a hertz.

4. The generator is short-circuit safe because it losses its excitation power, and restarts upon removal of the short. In connection with this, the variation in output voltage with load may be decreased by adding capacitance in series with the load.

5. Operation of the generator appears to be better self-excited. This is probably because the generator adjusts the current phase angles to minimize the loss mechanisms or optimize the performance within the terminal constraints. The generator appears able to do this better than an external operator or control system.

Other points to note are that the external capacitance on the three phases can be adjusted to balance the three phase currents, and that the fluid velocity or slip varies with the generator load but is almost independent of the setting of the series valve (provided that the velocity and pressure gradient are high enough to maintain self-excited operation). The powers for the three phases were not balanced, as for normal line operation, and optimizing the output power requires different load resistances on the three phases. It is interesting to note that the start of self-excited operation is not instantaneous, but usually requires a few seconds before anything happens.

The results from one self-excited case are shown in Table V. First note that this is a small generator (only about 6000 watts input power), and that there is no compensation of any kind for end loss. This case does not correspond to any that have yet been analyzed, and it was not clear to start with if self-excited operation could be attained from a one-wavelength-long generator without any end-loss compensation. Yet the efficiency for this case is reasonably good, and the performance is better than for the generator when connected to the power line. Using the simple theory shows that almost all of the input mechanical power can be accounted for as viscous loss, ohmic loss in the fluid, ohmic loss in the exciting winding, and output power. Only about 5% of the input power is not accounted for among the above, or goes into end loss or the other possible loss mechanisms. This would amount to a large fraction of the power at the low slips required for a generator with a high efficiency, so that more study of the performance at low slips is required.

TABLE V. Data From One Self-Excited Case.

MECHANICAL

v = 60.4 ft/sec

Total input power = 5780 watts

Viscous power loss = 1330 watts

ELECTRICAL

Frequency = 35.0 hertz v_s = 24 ft/sec

s = -1.5 R_M = 0.73 $1/R_M$ = 1.4

Phase currents = 25.8, 27.6, 27.8 amps

Phase voltages = 77 ½, 97 ¼, 86 ¼ volts

Output power = 870 watts

Total efficiency = 0.15

Electrical efficiency = 0.20 $\frac{1}{1-s}$ = 0.40

Coil loss = 610 watts

Generated power/net input power = 0.33

3.3.4 Harmonic Measurements

The harmonic content of one generator phase voltage was measured with a General Radio Model 1900A wave Analyzer for a variety of terminal conditions. The results are given in Tables VI and VII for operation both from the 60-hertz power line and self-excited, respectively. The numbers above the line set the terminal constraints, and the numbers below the line are the fundamental and harmonics of the terminal voltage, all in millivolts. The voltage measurements were made through a dropping resistor, so that only the relative sizes are significant. The main points are:

1. For the 60-hertz power-line cases the third and ninth harmonics may be reduced due to the delta-connected transformer back in the power system. Note that the harmonics increase as the phase current does, as expected since saturation is becoming more important. In none of these cases are harmonics significant, at most only a few per cent, or saturation is not very important. This means that the power level is limited by heating of the exciting coils and the available pump pressure rather than the iron.

2. The third harmonic is much larger for the self-excited cases as there is no delta-connected transformer. The largest phase current and highest harmonic content occurs for the seventh case. For this case there is no load resistance, and the third harmonic is about 15% of the fundamental. Adding load resistance, sixth case, decreases all harmonics greatly. The higher harmonics drop off faster for self-excited operation.

3. For all cases the even harmonics are negligible, as expected.

It is not certain for the self-excited cases where the drive for the harmonics comes from since the harmonics do not meet the frequency constraint imposed by the external capacitance. However, the harmonics apparently must be there because of the nonlinearities, or they are generated by the nonlinearities of the system. If the iron for a generator is pushed to its limit, saturation effects, and thus harmonics, could be very large. This point is important because the harmonics may cause excessive ohmic loss in the fluid besides affecting the operation of the associated power system.

TABLE VI: Harmonic content for 60-hertz line excitation.

Phase current, amps	20	20	20	30	30	40	40	45	45
Fluid velocity, ft/sec.	77.8	69.0	61.0	71.8	61.3	66.9	61.3	65.2	61.3
Component	Voltage in Millivolts								
Fundamental	9,250	9,400	9,400	14,100	14,200	18,300	18,300	20,200	20,300
2	~1 1/2	~ 4	~ 2	~ 3	~ 3	~ 5	~ 5	~ 5	~ 3
3	64	65	66	160	148	315	295	355	370
4	~ 4	~ 5	~ 2	~ 2	~ 5	~ 10	~ 8	~ 6	~ 10
5	64	63	66	110	120	193	203	186	172
6	~ 2	~ 7	~ 2	15	~ 3	~ 6	~ 4	~ 7	~ 15
7	13	15	12	20 1/2	21	28	27	22	31
9	~ 1.2	1.2	1.2	2.3	2.1	4	~ 5	4.6	5.4
11	7.8	7.2	6.2	8.4	8.6	14	15.8	15.6	15.2
13	3.2	3.4	3.2	5 1/2	4.8	6.6	5.4	6.8	6.2

TABLE VII: Harmonic content for self-excited operation.

Frequency, hertz	50.5	50.4	50.8	59.8	60.0	35.0	34.5	42.6	42.1
Phase current, amps	28.9	31.9	20.7	23.9	16.9	27.0	38		
Fluid velocity, ft/sec.	68.7	65.5	74.9	74.9	79.3	63.6	52.7	69.0	58.4
COMPONENT	VOLTAGE IN MILLIVOLTS								
Fundamental	12,500	14,200	9,100	12,600	8,900	8,250	11,800	8,850	13,300
2	0.6	∿1	∿1	<1	0.8	∿1	∿2.5	∿1	∿2.4
3	193	365	54	96	36	205	1,800	300	1.47
4	0.2	0.3	<0.2	<0.2	0.3	<0.2	<0.4	½	∿1
5	95	146	7.8	21	3.4	7.4	59.5	2.4	8.4
6	<0.2	0.2	0.2	<0.2	0.4	<0.2	<0.2	<0.1	<0.2
7	12.7	17½	2.05	13	3.2	0.85	13.6	0.7	8.4
9	1.8	4.4	0.4	2.1	0.5	0.65	13	0.25	5.4
11	0.7	2.2	<0.05	0.3	<0.1	<0.1	1.6	<0.1	0.6
13	0.3	0.4	<0.05	<0.2	<0.05	<0.1	0.6	<0.1	<0.2

3.3.5 Other Tests

Two other significant sets of tests have been run. First, a series of various hypothetical accidents were checked for self-excited operation, all at a frequency of 50.4 hertz and an undisturbed output power of 360 watts. For this three-phase generator the loss of any phase stopped the generator. This might not be true for a generator with a larger number of phases, and might not be true for this generator if the fluid velocity was allowed to pick up greatly during the accident. (This was limited by partially closing the series valve to prevent possible damage to the fluid channel.) Both opening one phase, as might occur if a fuse blows, and opening one leg of the main, delta-connected capacitor bank stopped the generator. A sharp increase in the load on one phase could be carried up to some threshold value, with the threshold value depending on the available extra flow capacity (or setting of the series valve). Using too small of a load resistance, approaching a short circuit, would stop the generator. The effect of changing the load resistance could be decreased by the use of series capacitance. (This was not checked experimentally.)

The second set of tests was to operate the machine in a two-wavelength version by reconnecting the coils, going from two slots per phase per pole to one slot per phase per pole. Here there is no equivalent of the symmetrical connection of the coils to reduce the effects of the open magnetic circuit. The main disadvantage, though, for the two-wavelength version is that for the same phase current there is only half as many ampere-turns per wavelength, or only half of the magnetic flux density. This means that the ohmic exciting loss is the same as for the one-wavelength version, but the generated power is one quarter of the original, as is R_M. Thus it was impossible to obtain self-excited operation or to produce net output power. Otherwise, the performance was similar and the phase currents were still unbalanced.

SECTION IV

CONCLUSIONS AND RECOMMENDATIONS

The results obtained from the operation to date of this generator are very encouraging. Self-excited operation and reasonable efficiency for a small generator have been obtained without difficulty. The control system and measurement system have worked adequately. These results indicate that end loss may not be as serious as first expected, but futher measurements are needed.

Now that the shake down procedures have been completed and excellent results obtained, there are several futher experiments which should be performed with the existing stator structure before the design and construction of a new stator. First, further study of end loss and compensation methods is required. A new, vaned channel is needed because of leaks in the original, and the compensating poles should be rebuilt (rewound) for further tests. Also, some of the points raised earlier, such as the harmonics when self-excited at high iron flux densities, should be examined in more detail as they may influence the system operation. Finally, a series of studies on a two-phase working fluid using the same stator is an important corollary to the above results as this will allow the comparison of the single and two-phase results without the complication of a different generator structure.

REFERENCES

1. Jackson, W.D., and Pierson, E.S., "Operating Characteristics of the M.P.D. Induction Generator," Magnetoplasmadynamic Electrical Power Generation, I.E.E. Conference Report Series No. 4, 38, 1963.

2. Elliott, D.G., "Two-Fluid Magnetohydrodynamic Cycle for Nuclear-Electric Power Conversion, ARS J, 32, 924, June 1962.

3. Brown, G.A., and Lee, K.S., "A Liquid Metal MHD Power Generation Cycle Using a Condensing Ejector," Proceedings of the International Symposium on Magnetohydrodynamic Electrical Power Generation, Paris, Vol. 2, 929, July 1964.

4. Petrick, M., "Liquid-Metal Magnetohydrodynamics," IEEE SPECTRUM, 2, 137, March 1965.

5. Prem, L.L., "Fluid Metal MHD-Steam Binary Plant Economy for Central Stations," Electricty from MHD, 1968, International Atomic Energy Agency, Vienna, 1968, Vol. III, 2005.

6. Radebold, R. et al., "Energy Conversion with Liquid Metal Working Fluids in MHD-Staustrahlrohr," Electricity from MHD, 1968, International Atomic Energy Agency, Vienna, 1968, Vol. III, 1439.

7. Boldyrev, V.M. et al., "Thermodynamic Analysis of New Cycles for Liquid-Metal MHD Generators," Electricity from MHD, 1968, International Atomic Energy Agency, Vienna, 1968, Vol. III, 1587.

8. Cerini, D.J., "Circulation of Liquids for MHD Power Generation," Electricity from MHD, 1968, International Atomic Energy Agency, Vienna, 1968, Vol. III, 2019.

9. Pierson, E.S., The MHD Induction Machine, Sc.D. Thesis, Department of Electrical Engineering, Massachusetts Institute of Technology, Cambridge, Massachusetts, September 1964; or AFAPL-TR-65-107, Research Laboratory of Electronics, Massachusetts Institute of Technology, Cambridge, Massachusetts, May 1966.

10. Pierson, E.S., and Jackson, W.D., Channel Wall Limitations in the MHD Induction Generator, ANL-7148, Argonne National Laboratory, Argonne, Illinois, March 1966.

11. Lielpeter, J.J., "Applicability of the Electrodynamic Approximation in the Theory of Liquid-Metal Induction MHD Converters," in Electricity from MHD, vol. 2, 1041, 1966.

12. Okhremenko, N.M., and Chepovetsky, "Optimum Geometric Relationships in a Coaxial Linear Induction-Type MHD Generator," Electricity from MHD, 1968, International Atomic Energy Agency, Vienna, 1968, Vol. III, 1935.

13. Weh, H. and Waltke, G., "Operating Characteristics of Electodeless MHD-Transducers with Regard to the Finite Length," Advanced Energy Conversion, 5, 147, 1965.

14. Peschka, W., Kelm, S., and Engeln, F., "Penetration Effects at the MHD Induction Engine of Semi-infinite Length," in Proceedings of the International Symposium on Magnetohydrodynamic Electrical Power Generation, Paris, vol. 2, 917, July 1964.

15. Prem, L., Rowe, I., and Mouradian, E.M., Alternating Current Induction MHD Generator Research, AFAPL-TR-68-91, Atomics International, July 1968.

16. Elliott, D.G., "Variable-Velocity MHD Induction Generator with Rotating-Machine Internal Electrical Efficiency," Proc. IEEE, 56, 1449, 1968.

17. Discussion for Section 2-d, Design and Performance Studies, Electricity from MHD, 1968, International Atomic Energy Agency, Vienna, 1968, Vol. VI, 3709.

18. Pierson, E.S., Brown, G.A., and Jackson, W.D., Liquid Metal Magnetohydrodynamics, AFAPL-TR-69-33, Air Force Aero Propulsion Laboratory, Air Force Systems Command, Wright-Patterson Air Force Base, Ohio, May 1969.

19. Elliott, D.G., private correspondence.

20. Moody, L.F., "Friction Factors for Pipe Flow," Trans. Amer. Soc. Mech. Engrs., 66, 671, 1944.

21. Cerini, D.F., and Elliott, D.G., "Performance Characteristics of a Single-Wavelength Liquid-Metal MHD Induction Generator with End-Loss Compensation," Proceedings of the Eight Symposium on Engineering Aspects of Magnetohydrodynamics, Stanford, California, 1967, 11.

22. Moszynski, J.R., Reduction of Electrical End Losses in MHD Generator Channels by Insulating Vanes, ANL-7188, Argonne National Laboratory, Argonne, Illinois, 1967.

23. Pierson, E.S., and Jackson, W.D., "Experimental Study of a One-Wavelength MHD Induction Generator," Proceedings of the Tenth Symposium on Engineering Aspects of Magnetohydrodynamics, M.I.T., Cambridge, Mass., March 1969, pp. 53-57.